Oxidation of SiC$_f$-SiC CMC cladding tubes for GFR application in impure helium atmosphere and materials interactions with tantalum liner at high temperatures up to 1600°C

M. Steinbrueck[1], V. Angelici Avincola[1,3], I.J. Markel[1], U. Stegmaier[1], U. Gerhards[2], H.J. Seifert

[1] *Karlsruhe Institute of Technology, Institute for Applied Materials*
[2] *Karlsruhe Institute of Technology, Institute for Micro Process Engineering*
Hermann-von-Helmholtz-Platz 1, 76344 Eggenstein-Leopoldshafen, Germany
[3] *now with MPR Associates, Inc., Alexandria, VA 22314, USA*
email: martin.steinbrueck@kit.edu

The oxidation kinetics of SiC$_f$-SiC cladding tube segments and sandwich tubes with an inner tantalum layer in impure helium atmosphere prototypical for GFRs was investigated at ambient pressure in the temperature range between 900°C and 1600°C using a thermogravimetric device. The transition from passive oxidation (formation of a protective silica scale) to active oxidation (volatilization of silica due to the formation of SiO and other volatile species) occurred between 1200°C and 1300°C. Hence, during target operational temperatures of 900-1000°C, the CMC cladding material should withstand long-term operation with respect to oxidation and corrosion. At higher temperatures beyond 1300°C, i.e. under accident conditions, volatilization of composite constituents would lead to serious degradation of the SiC-based cladding tubes. Severe interactions between the tantalum layer and silicon carbide with the formation of Ta silicides and carbides were found to become significant at temperatures higher than 1300°C.

1. INTRODUCTION

SiC$_f$-SiC ceramic matrix composites (CMCs) are promising materials for cladding tubes for fuel assemblies in nuclear reactors. They consist of silicon carbide fibers, a weakly bonded interphase made of PyC, and a matrix of SiC e.g. chemical vapor infiltrated and may include a dense external CVD SiC layer. Their excellent stability at high temperatures makes them a favorable candidate for application in gas-cooled fast reactors (GFR). The expected GFR operating conditions are in helium as coolant at a pressure of 8 MPa, temperatures up to 1000°C, and gas flow as high as 90 m/s. Although the helium is expected to be of high purity, a low amount of impurities like oxygen, water, nitrogen, and others, is unavoidable in a technical system like a nuclear reactor. Especially the oxidizing impurities bear the risk of oxidation and corrosion of the cladding tubes during long-term operation under the extreme conditions.

In the framework of the FP7 MatISSE project [1] the high-temperature oxidation and corrosion behavior was experimentally investigated under operation and accident conditions prototypic for a GFR. This paper presents a summary of results obtained at Karlsruhe Institute of Technology (KIT) on high-temperature oxidation of SiC$_f$-SiC tube segments in flowing helium with GFR coolant chemistry at temperatures between 900°C and 1600°C at ambient pressure. The samples were produced and provided by the French Alternative Energies and Atomic Energy Commission (CEA). The impurities content of helium proposed by the UK National Nuclear Laboratory (NNL) and agreed within the MatISSE working group is based on a literature survey [2] and it reflects the He coolant conditions reported from the Chinese HTR-10 prototype reactor, which has been also used as a reference environment for the demonstrator ALLEGRO. First results of this work concentrating on the oxidation of SiC$_f$-SiC at lower temperatures were already published by Avincola [3]. Fitzgerald's review paper [2] discusses in detail the state of knowledge on high-temperature corrosion and erosion of silicon carbide. Hence, in this chapter only a brief summary of the most important phenomena and reactions is given.

The oxidation of SiC can be divided into so-called passive and active oxidation. The excellent high-temperature resistance of silicon carbide is based on the formation of a passivating silica scale according to Eqs. 1-3, and described by parabolic correlations; i.e. the mass gain or oxide scale growth rates are proportional to the square root of the time. The rate determining step of the oxidation process at the SiC/SiO$_2$ interface (described by reaction 1a,b, 2, and 3) is the diffusion of the oxidizing species through the silicon oxide scale, once homogeneously formed on the SiC substrate. Before this stage, a linear oxidation law could be observed, as it is directly determined by

the interface reaction. In presence of H_2O, reaction (2) is likely dominating, as it is faster than reactions 1a,b. CO_2 is another potential oxidizing agent, and reacts with SiC according to Eq.3.

$$SiC + 2O_2 \rightarrow SiO_2 + CO_2 \tag{1a}$$

$$SiC + 1.5O_2 \rightarrow SiO_2 + CO \tag{1b}$$

$$SiC + 3H_2O \rightarrow SiO_2 + 3H_2 + CO \tag{2}$$

$$SiC + 3CO_2 \rightarrow SiO_2 + 4CO \tag{3}$$

At high temperature and low oxidant partial pressure the so-called active oxidation takes place, with the formation of volatile SiO instead of the protective silica (Eq.4). The transition between active and passive oxidation is determined by temperature and partial pressure of the oxidizing species [4] [5] [6]. The mass loss by this reaction is usually described by linear kinetics.

$$SiC + O_2 \rightarrow SiO + CO \tag{4}$$

In water/steam containing atmosphere, the formation of volatile silicon hydroxides additionally contributes to the degradation of the silica scale at high temperatures and high flow rates, mainly following Eq.5 [7] [8]. Growth and volatilization of the oxide scale can be described by a paralinear oxidation model [7].

$$SiO_2 + 2H_2O \rightarrow Si(OH)_4 \tag{5}$$

The oxidation behavior of SiC_f-SiC CMCs, as well as the oxidation of the PyC interphase [9] [10] (if exposed to the atmosphere) has to be assessed in order to understand and predict the oxidation/corrosion behavior of the composite. Moreover, the interaction between SiC and the inner tantalum layer used in so called sandwich tubes is still unknown under GFR conditions to the best of the authors' knowledge.

This paper presents the outcome of an extensive experimental program on the high-temperature oxidation behavior of SiC_f-SiC, sandwich samples with internal tantalum tubes in impure helium at normal pressure. Additionally, in the framework of MatISSE, experiments on SiC_f-SiC corrosion and erosion under high pressure and high flow rates obtained in a helium loop were conducted at Research Centre Rez (CVR). Results of this experimental program will be published elsewhere.

2. EXPERIMENTAL DETAILS

2.1. Test facility and conduct

All oxidation experiments were performed in a symmetric thermal balance Setaram TAG 16/18 Evo [11]. The symmetric design with two furnaces, one for the sample and one for the

reference, allows highly precise mass change measurement without the need of reference tests for buoyancy correction. Two gas mixtures (He+H_2O; He +other impurities) were injected through the balance case as well as above the sample and mixed in the reaction tube; the gas flow was from top to bottom. The oxygen concentration of the off-gas was measured using a ZIROX [12] oxygen analyzer with an yttria stabilized zirconia solid electrolyte. An alumina tube segment of similar size like the SiC samples was used as reference sample. The thermocouples (TC, type S) were located very near below the samples without contacting it. After several failures of the Pt-Rh TCs due to the hydrogen and CO containing atmosphere, the thermocouples were protected by a one-side closed alumina tube. This measure did not affect the temperature control during the isothermal experiments.

Each sample was weighed before and after the test. Once inside the thermo-gravimetric (TG) system, the samples were heated to the predefined temperature with a rate of 30 K/min in pure (99.9999%) helium. After thermal equilibration at this temperature for 300 s the helium gas with prototypical impurities according to Table 2 was introduced. All tests performed were isothermal ones, with typical duration of 3, 20, 200, and 1000 h, respectively.

At temperature lower than 1200°C a Pt wire was used to hang the sample in the furnace. Beyond 1200°C, due to the aggressive attack of the atmosphere, the platinum was replaced by ceramic sample holders and a suspension system made of alumina. To account for the SiO evaporated from the sample and condensed on the sample suspension, the TG measurements were corrected for the calculation of rate constants using the initial and post-test masses determined with a separate laboratory balance.

2.2. Specimens and gas atmosphere

Altogether six types of samples (SiC$_f$-SiC with and without tantalum liner, three surface qualities each) were investigated. All samples were manufactured and provided by CEA [13]. The dimensions were 10 mm length, and outer/inner diameters of 9.50/7.80 mm and 9.75/7.75 mm for SiC$_f$-SiC and sandwich samples, respectively. The samples had three different surface roughnesses (Ra) and were named: "as-manufactured" ($R_a \approx 50$ μm), "ground" ($R_a \approx 10$ μm) and "smooth" ($R_a \approx 2$ μm). Ground samples are as-manufactured sections that were subjected to mechanical grinding and then overcoated with β-SiC by PVD. Smooth samples are ground sections that were subjected to an additional mechanical grinding. For the analyses of TG results the geometrical surfaces of all samples were determined. The real surface of the samples should be different for the

three types of surface quality. This issue has to be taken into account during the discussion, although the difference should not play a major role in the interpretation of the results.

The SiC$_f$-SiC samples were prepared by CEA from high purity Hi-Nicalon S SiC fibers by 2D filament winding (first layer) and 2D braiding (2nd and 3rd layer). The fibers are covered by a 30-50 nm pyrocarbon (PyC) interphase. The SiC matrix was produced by chemical vapor infiltration (CVI) process, also resulting in high-purity SiC. The sandwich samples additionally contained a 0.1 mm tantalum liner between the first and second layer. After cutting, all samples received a CVD SiC coating in order to seal SiC fibers and Ta liner. Table 1 gives an overview of samples investigated and Fig. 1 shows macro and micro views of the as-received SiC$_f$-SiC samples. The different surface qualities are clearly seen in the macrographs and SEM images of Fig. 1.

The helium gas mixture used was purchased from AIR LIQUIDE with a composition prototypic for a GFR. The impurity concentrations for these experiments at normal pressure were scaled in order to obtain the same partial pressures as in a GFR at 70 bar operating pressure as shown in Table 2. Due to practical reasons, two mixtures had to be used, one with water as the only additive and a second with all other impurities. Both gases were mixed 50/50, i.e. the purchased gas mixtures had to contain the double impurity concentrations compared to the values given in Table 2. Furthermore, the maximum available water concentration in helium was 120 vppm, so the finally applied water concentration was 10 vppm lower (60 vppm) than predefined. The gas flow rate for all experiments was kept constant at 30 ml/min (total flow) resulting in a flow velocity of approx. 8 cm/min.

Table 1: Overview of samples investigated

Sample	Type	Surface
L1	SiC$_f$-SiC	as manufactured
L2	SiC$_f$-SiC	ground
L3	SiC$_f$-SiC	smooth
SL1	sandwich	as manufactured
SL2	sandwich	ground
SL3	sandwich	smooth
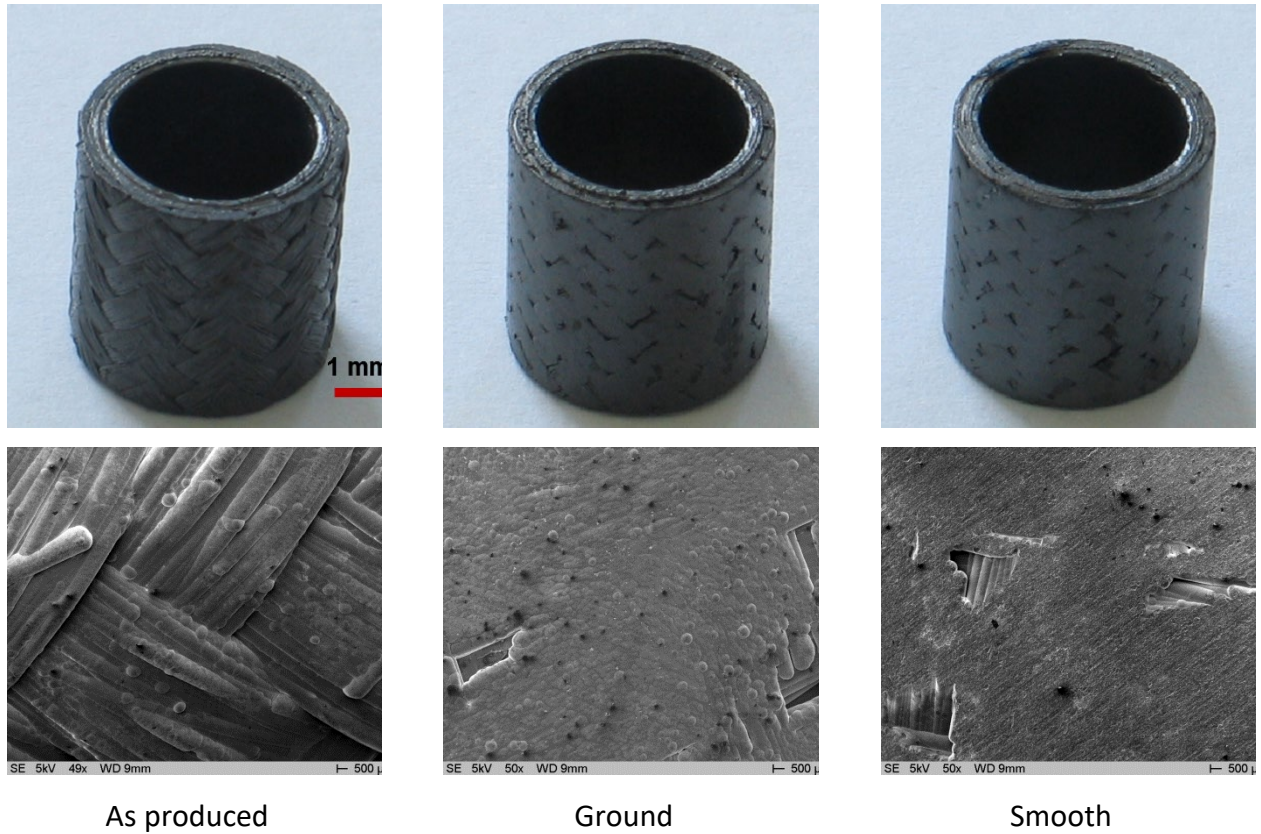
Fig. 1: SiC$_f$-SiC samples. First row: Macro appearance of the surface. Second row: SEM images of the surface.

Table 2: Impurity composition of the helium gas used

Impurity	Concentration at 70 bar vppm	Concentration at 1 bar vppm	Applied concentration vppm
H$_2$	3	210	210
CO	3	210	210
N$_2$	2	140	140
O$_2$	1	70	70
H$_2$O	1	70	60
CH$_4$	1	70	70
CO$_2$	1	70	70

The gas mixture is of strongly reducing character due to its high contents of H$_2$ and CO. The calculated equilibrium composition depending on temperature is given in Fig. 2. In the linear scale no oxygen is seen; the oxygen equilibrium compositions at 500, 1000, and 1500°C are 10^{-27}, 10^{-13}, and 10^{-7} mol%, respectively. The results of the equilibrium calculations are theoretical values. The real gas composition may differ from these values e.g. due to kinetic limitations in this strongly diluted gas mixture, especially at lower temperatures.
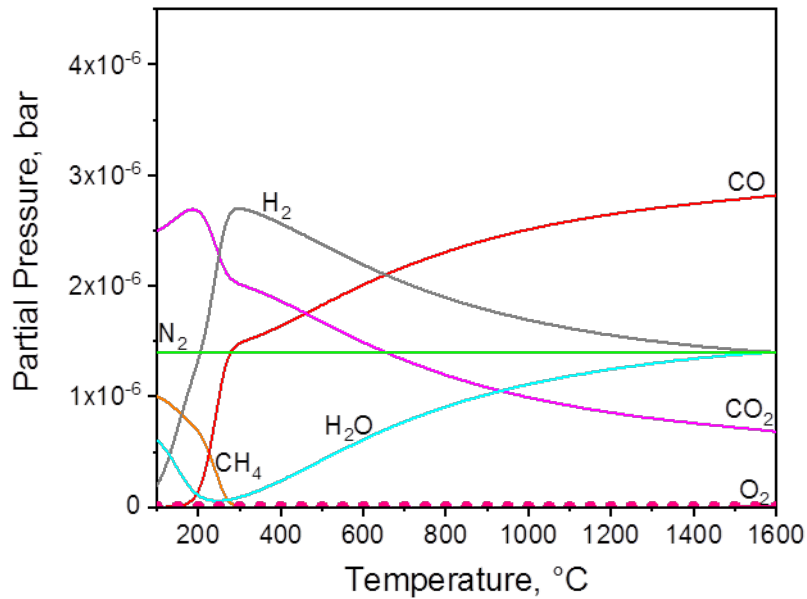
Fig. 2: Equilibrium gas composition of the applied gas mixture helium plus impurities as given in Table 2 calculated with Thermo-Calc [14] using the data base from SGTE [15]

2.3. Post-test examinations

After the experiment the post-test masses of the samples were determined and macro photos were taken to document the appearance of the SiC tube segments before embedding them. The surface of some samples was documented and analyzed by SEM/EDX as well. Scanning electron microscopy was performed with a Philips XL30S FEG with field emission gun equipped with a silicon drift detector (SDD) for element analysis. Element analyses and line-scans where performed at 5 kV acceleration voltage to achieve best possible results in regard to the light elements. The local composition of the SiC-Ta interaction zone for selected sandwich samples was analyzed by a JEOL JXA-8530F Field Emission Electron Probe Microanalyzer (EPMA) with 10 kV acceleration voltage and 20 nA probe current.

2.4 Thermodynamic Modelling

CALPHAD-type [16] equilibrium calculations were performed, using the Thermo-Calc software [14], to support and explain the conducted experiments.

The equilibrium composition of the prototypical GFR atmosphere (He+Impurities) was calculated in the experimentally covered temperature range. Furthermore the transition from passive to active oxidation of SiC in this specific atmosphere was determined. Calculations were performed using thermodynamic descriptions of the gas species from the SGTE substance database

SSUB v4.1 [15]. Additionally, data for the binary systems Si-C [17] and Si-O [18] were added from literature. Interactions of the inner Ta layer with the SiC-based cladding tube were investigated and discussed on the basis of the isothermal section in the ternary Ta-Si-C system at 1500 °C and the temperature-composition diagram across the SiC-Ta interface. The thermodynamic dataset for the ternary system Ta-Si-C was deduced by extrapolation from the binary subsystems Si-C [17], Si-Ta [19] and Ta-C [20]. Carbon solubility in Ta_5Si_3 is known from literature [21] as for other Me_5Si_3 silicides [22]. However no $Ta_5Si_3C_x$ phase was introduced to the present dataset as its carbon content is under ongoing discussion [23] and no conclusive thermodynamic description is available in literature.

3. EXPERIMENTAL RESULTS

3.1 Oxidation of SiC$_f$-SiC samples

Oxidation tests with SiC$_f$-SiC (non-sandwich) samples were conducted at temperatures of 900, 1000, 1200, 1300, 1400, 1500, and 1600°C, respectively, mostly for 20 hours. Longer duration tests have been performed additionally for 200 h at 1000°C and 1000 h at 900°C and 1200°C, shorter durations of 3 hours for experiments at very high temperatures of 1400-1600°C.

3.1.1 Thermo-gravimetric results

The mass change data of all tests were referred to the geometrical surface of the samples for the sake of comparison with literature data. Fig. 3 gives an overview of mass changes measured for all temperatures with one typical sample per temperature and sample type in a 20-hours time scale. The diagram shows original data shifted to the (0,0) position for initiation of the gas injection, but without further corrections for the determination of kinetic constants as discussed below. At a first glance the most important outcome of the experiments is visible: linear mass loss regime, i.e. active oxidation of the SiC$_f$-SiC samples occurs at temperature higher than 1200°C. At temperatures between 900 and 1200°C mass gain is observed suggesting that passive oxidation due to the formation of a silica scale took place. As noted in Fig. 3, both effects increase with increasing temperatures, especially the mass losses increase dramatically with increasing temperature.

The three different sample types (as manufactured, ground, smooth) behave slightly different, especially in the temperature range of passive oxidation. In general, it can be stated that the mass changes at temperatures 900-1200°C are very low as seen in the diagrams of Fig. 4 to Fig. 5, reaching the resolution limit of the TAG system. Nevertheless, there seems to be a reproducible effect of the surface quality on the initial phase of the oxidation. At 900°C as well as at 1200°C (Fig.

4) mass gain starts immediately after initiation of the gas injection for the as-manufactured and ground samples whereas an initial mass loss is observed for the smooth samples before mass gain is established. This may be connected with the initial oxidation of grinding/polishing agents or of bare fibers with PyC layers leading to the formation of volatile CO/CO_2. A reference curve (shown in Fig. 4) obtained at 900°C with an inert alumina sample indicated that the sample effects are slightly overlapped by the system behavior of the TAG working in a not air-conditioned lab.
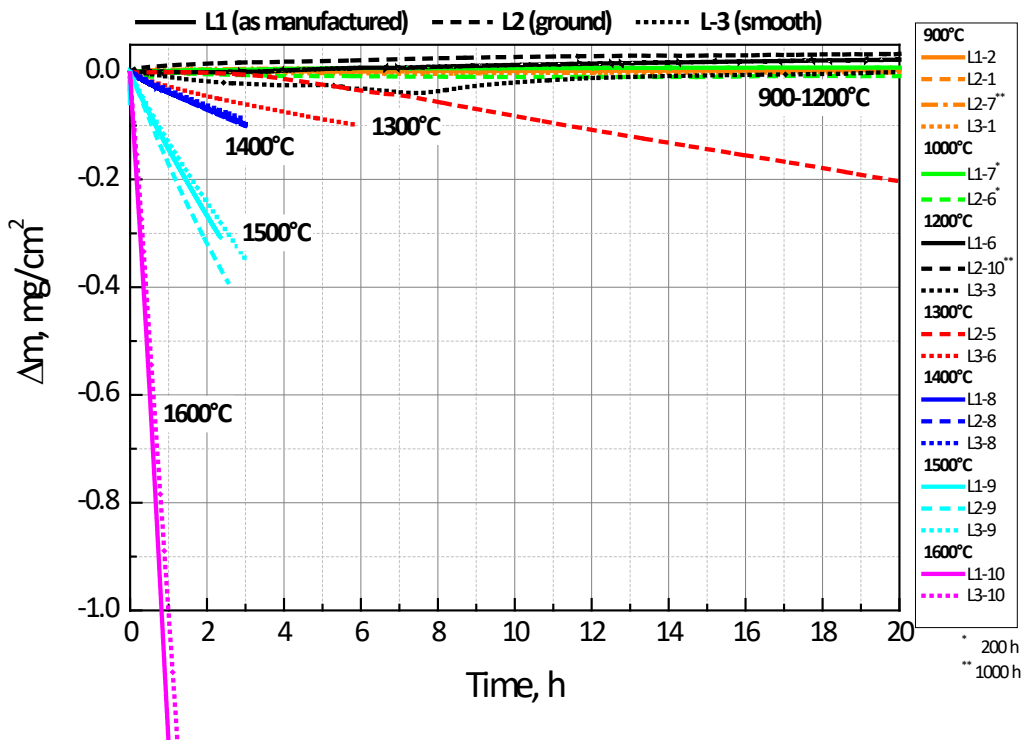
Fig. 3: Mass change during oxidation of SiC_f-SiC cladding tube segments in impure helium atmosphere at temperatures between 900 and 1600°C.

Interestingly, the mass gain of the ground samples is higher than of the as-manufactured ones, even one should expect a lower effective surface of the ground tube segments. Differences in mass loss of the samples were also observed for the higher temperatures but without any evident correlation. Therefore, these differences were taken as scatter of the corrosion behavior from sample to sample.

The longer duration tests with 1000 h annealing time shown in Fig. 5 demonstrated that after an initial mass gain for approx. 50-100 h the mass stabilized at an almost constant value (at least referred to the resolution limit of the balance).
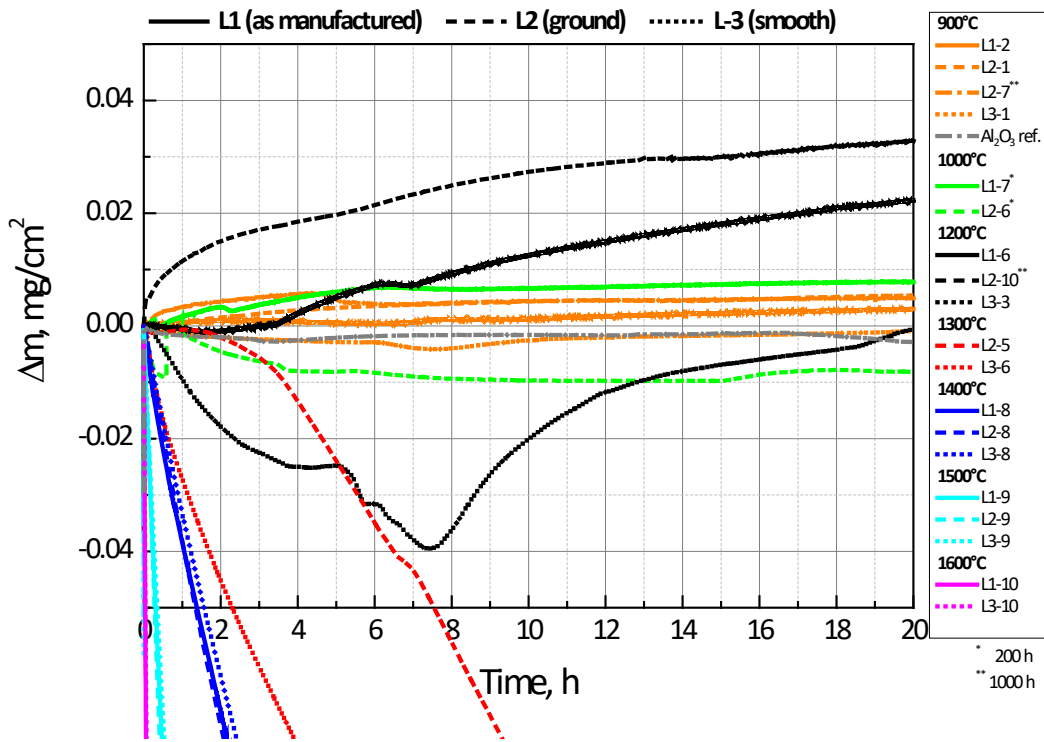
Fig. 4: Mass change during oxidation of SiC$_f$-SiC cladding tube segments in impure helium atmosphere at temperatures between 900 and 1600°C. Zoom on the 900-1200°C experiments with passive oxidation and one reference test at 900°C with Al$_2$O$_3$.
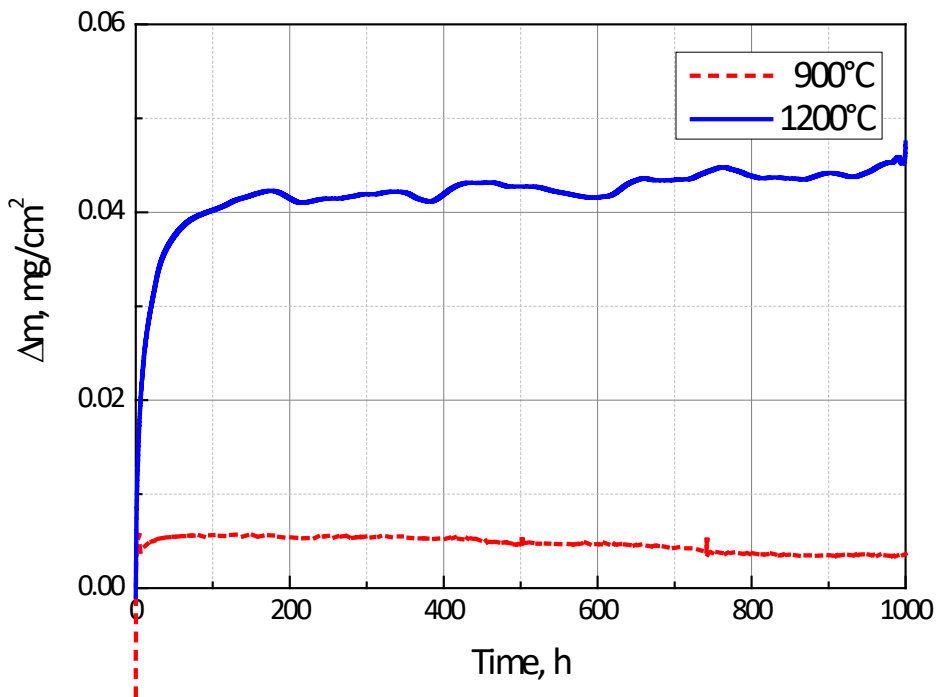
Fig. 5: Mass change during 1000 hours oxidation of SiC$_f$-SiC cladding tube segments in impure helium atmosphere at 900 and 1200°C

Kinetic data of the corrosion rates of the SiC$_f$-SiC samples can be obtained by fitting the TG curves to Eq.6.

$$\frac{\Delta m}{S} = K \cdot t^n \tag{6}$$

with Δm – mass change, S – surface of the sample, K – rate constant, t – time, and n – rate exponent. The exponent is n=1 for linear kinetics and n=1/2 for parabolic kinetics.

Table 3 summarizes the data used for the calculation of the linear mass loss rate constants including the corrected data taking into account volatilization and condensation on the sample holder as mentioned in chapter 2.1.

Table 3: Linear mass loss rate constants corrected by the ratio of the mass losses obtained by the TAG system and by an analytical balance. Note that the corrected rates have a different unit for better comparability with values given in literature, e.g. [2].

Sample	Temp. °C	Rate mgcm^{-2}h^{-1}	Δm(TAG) mg	Δm(bal.) mg	Corr. Rate mgcm^{-2}min^{-1}
L2-5	1300	-0.012	-1.16	-1.31	-2.26E-4
L3-6	1300	-0.014	-0.098	-0.11	-2.62E-4
L3-8	1400	-0.028	-0.503	-0.98	-9.09E-4
L1-8	1400	-0.0298	-0.557	-0.95	-8.47E-4
L2-8	1400	-0.032	-0.572	-1.1	-1.03E-3
L2-9	1500	-0.152	-2.19	-1.55	-1.79E-3
L3-9	1500	-0.112	-1.97	-2.3	-2.18E-3
L1-9	1500	-0.128	-0.55	-1.18	-4.58E-3
L1-10	1600	-1.79	-191	-85.5	-1.34E-2
L3-10	1600	-1.54	-125	-89.6	-1.84E-2

The Arrhenius diagram in Fig. 6 confirms that the high-temperature corrosion of the SiC samples is a thermally activated process. The temperature dependence of the reaction can be described by the following equations (Eqs.7), giving the activation energy as E_A = 326 kJ/mol.

$$\ln (K_l) = 16.45 - \frac{325677}{RT} \tag{7a}$$

$$K_l = 1.39 \cdot 10^7 \cdot \exp\left(\frac{-325677}{RT}\right) \tag{7b}$$
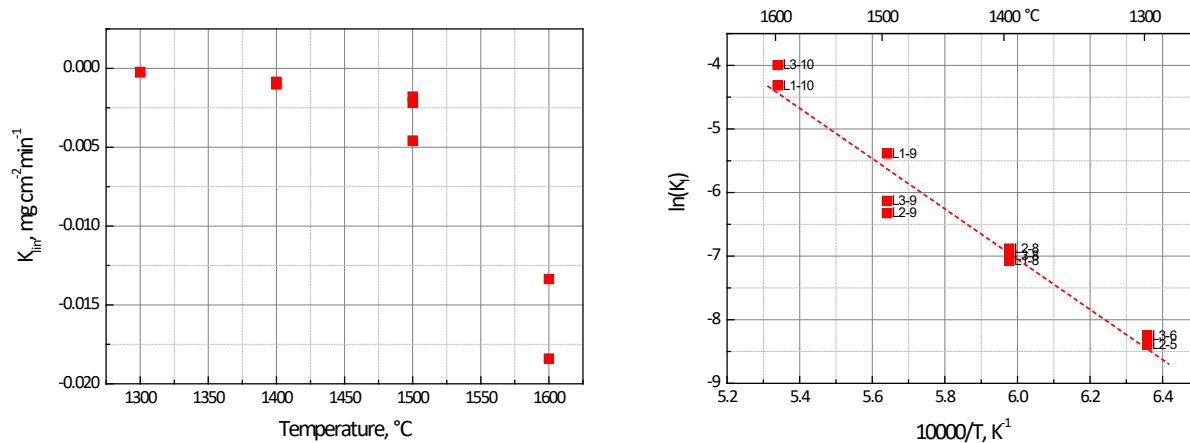
Fig. 6: Linear mass loss rates of the reaction of SiC$_f$-SiC with helium impurities at temperatures from 1300 to 1600°C. Left: Linear scale, right: Arrhenius diagram.

The evaluation of the experiments in the passive oxidation regime at lower temperatures is less straight forward. First, the mass changes are very small, for many tests at or even below the resolution limit of the analytical balance used, and second, the masses determined by TG are not changing homogeneously. However, the log(Δm/S)=f(log(time)) diagram of the two long-term tests at 900 and 1200°C (Fig. 7) allows to draw some conclusions. The exponent n of Eq. (6) corresponds to the slope of the log-log curves. The 900°C curve gives no relevant information, whereas for the 1200°C curve, three different regions can be distinguished. In the initial phase of the first ten hours a sub-parabolic behavior with n=0.37 is observed. Later on, up to approx. 100 hours, the exponent is reduced to n=0.14 and after 100 hours until the end of the test to n=0.035. This means that the long-term oxidation cannot be described by purely parabolic kinetics. For 900°C, the maximum operation temperature of a GFR, no significant degradation of the SiC$_f$-SiC cladding is expected at normal pressure and low flow rates even for long-term use, according to the extrapolation of the experimental data of this work.
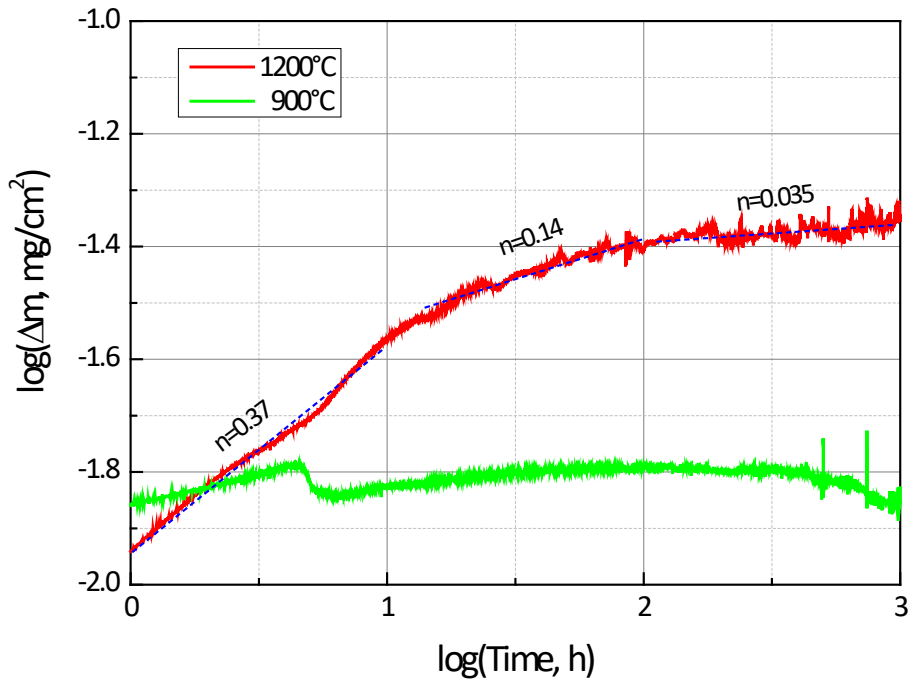
Fig. 7: log-log diagram of the mass change during the two experiments for 1000 hours at 900 and 1200°C.

3.1.2 Post-test examinations

The post-test appearance of almost all samples was documented by macro photos. A selection of photos taken after tests at various temperatures is presented in Fig. 8. At first glance, it can be seen that all samples kept their shape and are in mechanically stable condition; i.e. no obvious cracks or spallation is visible. Mechanical properties of these samples were not determined. Up to 1500°C only slight changes of the surface color are visible. The temper colors of the samples annealed at 900°C and 1200°C indicate very thin (sub-µm) oxide scale thickness. The sample annealed at 1600°C shows the formation of a white surface layer.

A deeper insight into the surface structure of the samples was obtained from SEM images shown in Fig. 9. A surface layer with increasing grain size is formed between 900°C and 1200°C. This layer is analyzed by EDX to be SiO_2, Fig. 10. The silica scale is in the sub-micrometer range at both temperatures, approx. 0.2 and 0.6 µm for the 1000-hours tests at 900°C and 1200°C, respectively. From 1300°C (not shown in Fig. 9) the surface is increasingly attacked by the impurities of the helium gas. Holes and craters are seen at the surface of the sample annealed at 1400°C and 1500°C. A much more serious attack deep into the bulk is observed for the sample annealed at 1600°C. The surface is heavily jointed (ragged) which should be the reason for its white appearance. The

remaining material is of cauliform structure. No superficial oxide scale was observed from temperatures of 1300°C and beyond; see e.g. bottom images of Fig. 10.

| **L2-7, 1000h, 900°C** | **L3-7, 200h, 1000°C** | **L2-10, 1000h, 1200°C** |

| **L2-8, 3h, 1400°C** | **L2-9, 2.6h, 1500°C** | **L1-10, 20h, 1600°C** |
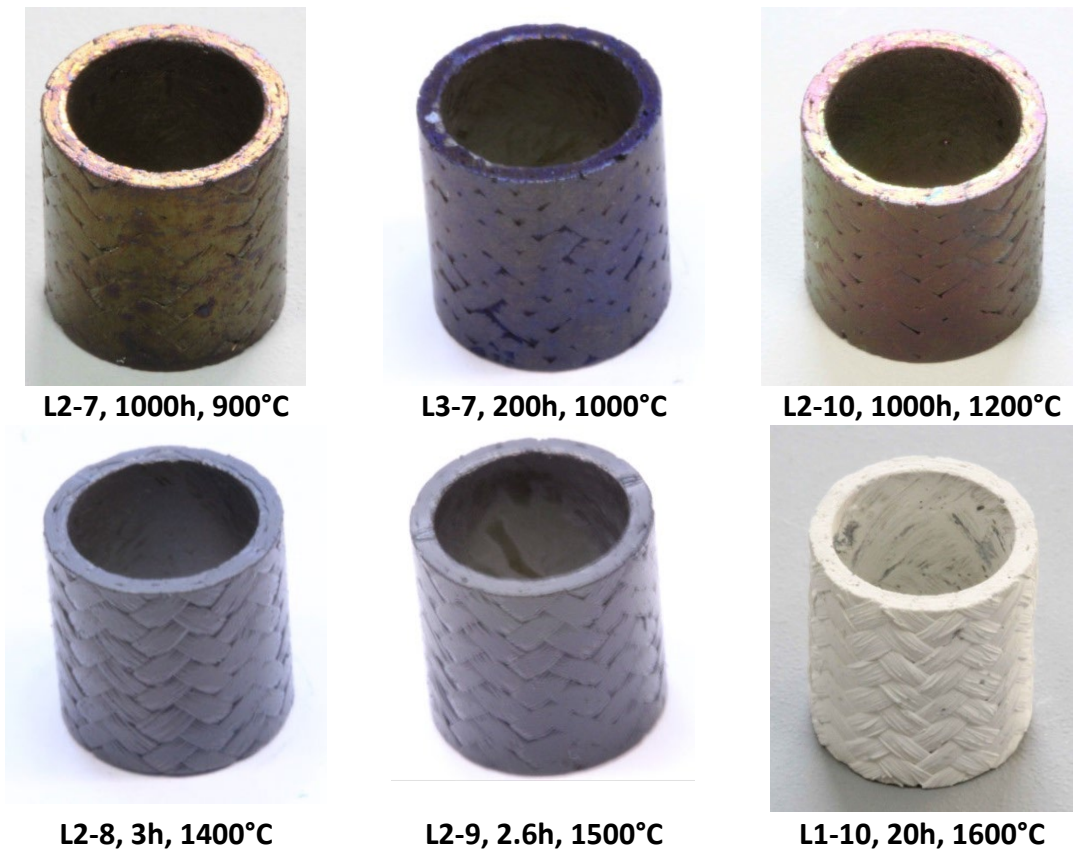
Fig. 8: Macro appearance of selected samples after oxidation tests in impure helium at various temperatures.
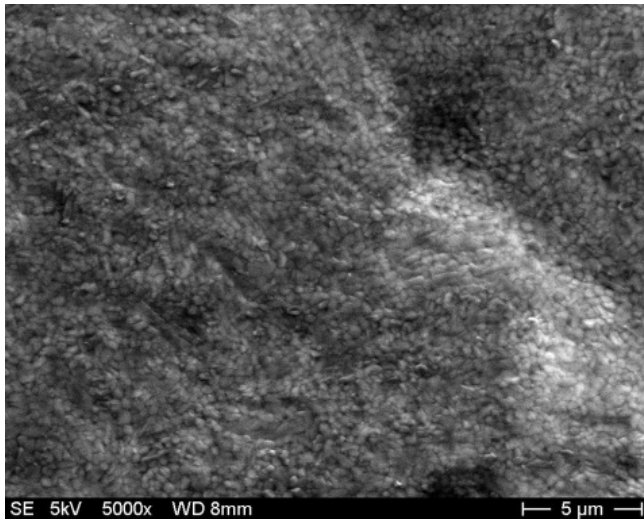
L2-7, 1000h, 900°C
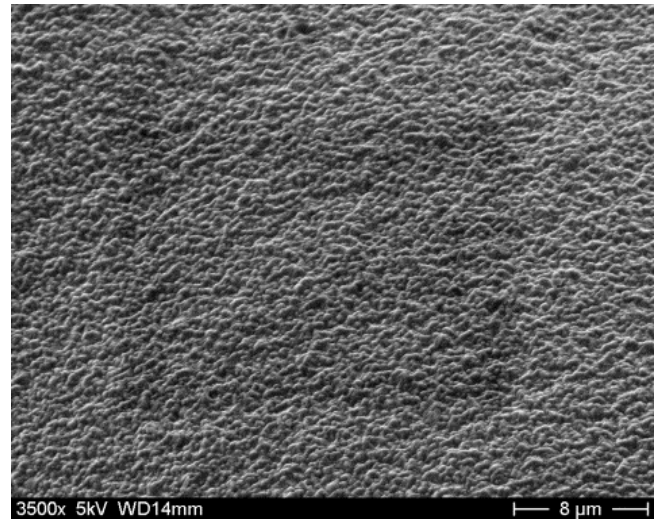
L3-7, 200h, 1000°C
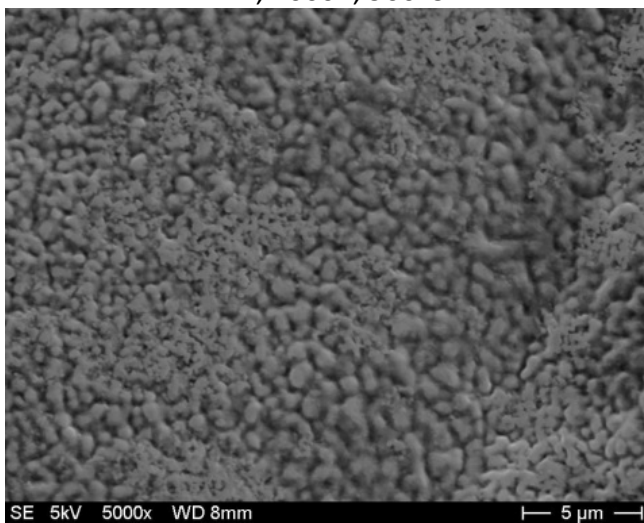
L2-10, 1000h, 1200°C
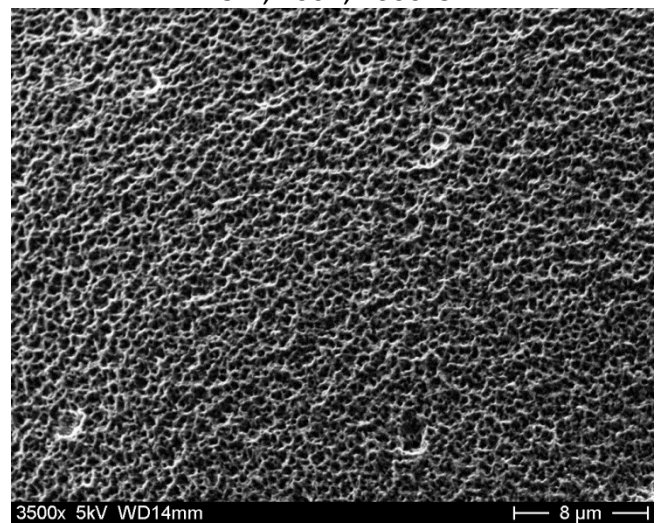
L2-8, 3h, 1400°C
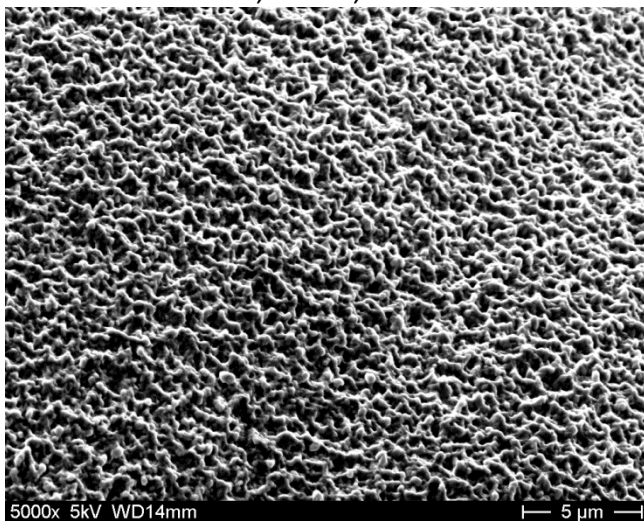
L3-9, 3h, 1500°C
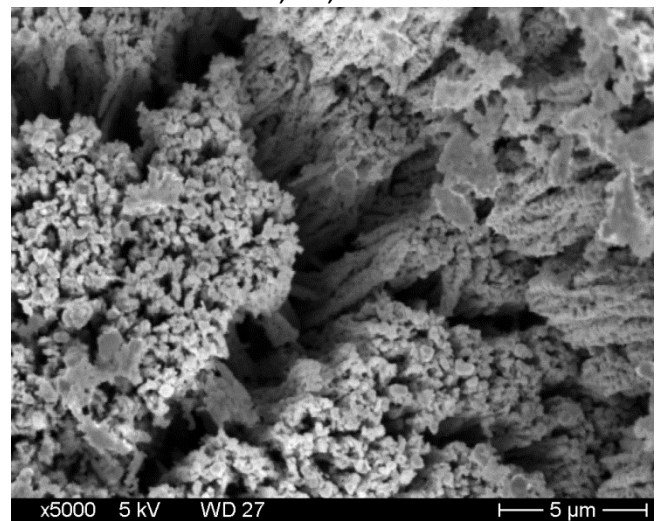
L1-9, 2.5h, 1600°C

Fig. 9: SEM surface images of selected samples after oxidation tests in impure helium at various temperatures and times.
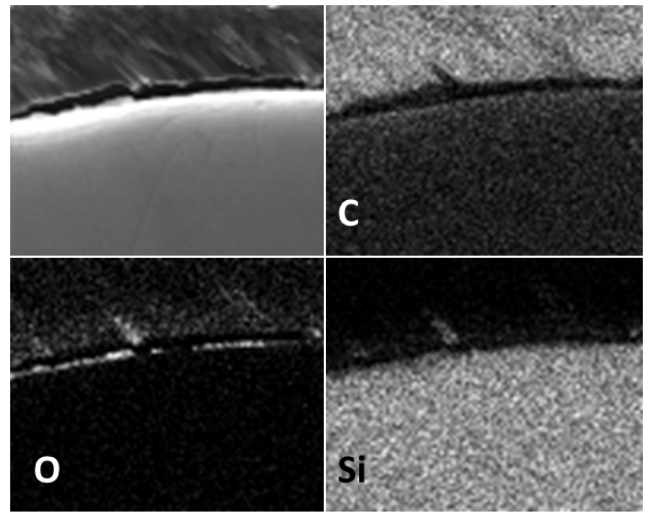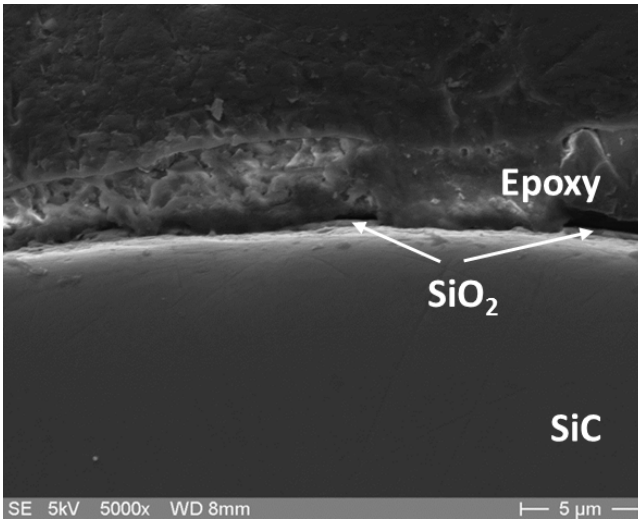
Sample L2-7 (1000 h at 900°C) showing the formation of a 0.2-0.3 µm thick SiO$_2$ scale.
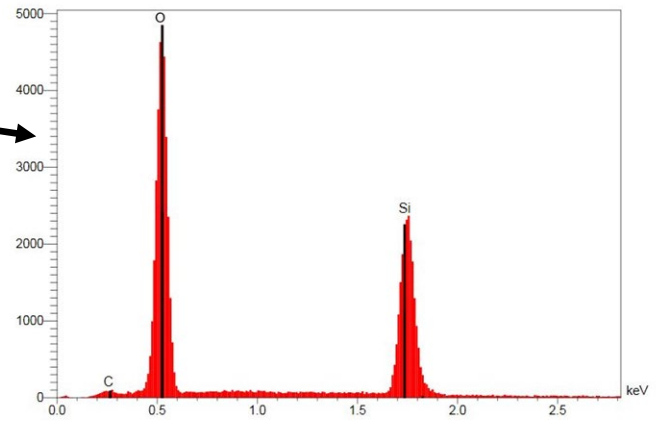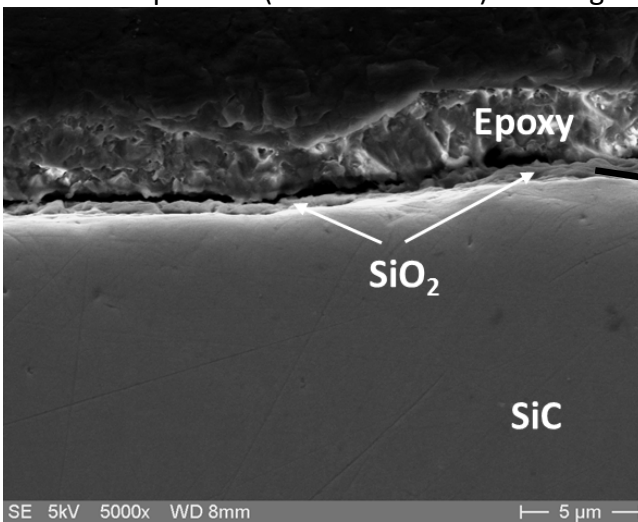
Sample L2-10 (1000h, 1200°C) showing the formation of a 0.5-0.7 µm thick SiO$_2$ scale.
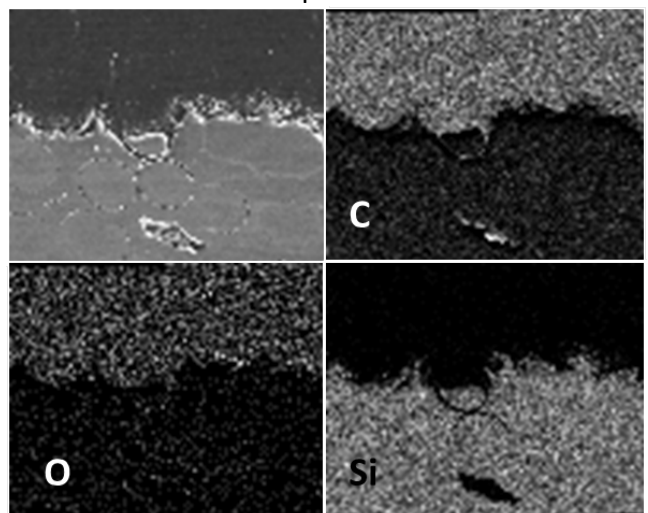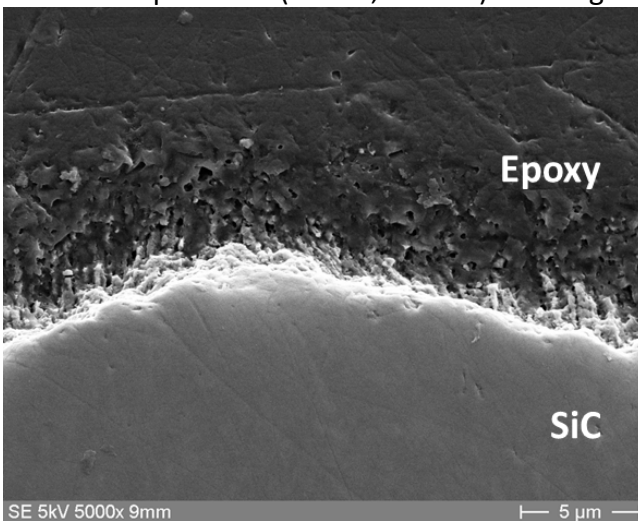
Sample L3-10 (20h, 1600°C) showing the absence of superficial SiO$_2$ scale
Fig. 10: SEM images and EDX results of cross sections of samples oxidized at various temperatures.

Additional EDX point analyses of the surface of the samples annealed at the highest temperatures show a reduced carbon content of the surface which may be explained by the preferred reaction of carbon forming volatile carbon-containing gases.

Generally, the SiC fibers with PyC coating were not attacked during the oxidation/corrosion tests. Only one example for a fiber attack was found at sample L3-10, annealed for 20 hours at 1600°C. SEM micrograph and corresponding EDX mappings for carbon and silicon have shown the consumption of the PyC coating of the fibers in contact with the oxidizing atmosphere. At lower temperatures no attack of fibers was observed at all.

The results obtained by these post-test investigations are in accordance with the TG-results; they confirm the transition from passive to active oxidation in GFR prototypic gas mixture between 1200°C and 1300°C.

3.2. Oxidation of sandwich samples with inner tantalum liner

Due to partial oxidation of the tantalum liner at the samples' edges the mass change curves were not meaningful and are not further discussed here. The general features were the same as for the non-sandwich samples with transition from passive to active oxidation at temperatures above 1200°C. The tantalum liner is easily oxidized after getting into contact with the atmosphere.

3.3. High-temperature interactions between silicon carbide and tantalum

The post-test examinations of the sandwich samples focused on the behavior of the tantalum layer during annealing, especially on its interaction with the surrounding silicon carbide. Selected optical micrographs of whole tube wall cross sections as well as of magnified regions of the tantalum layer are summarized in Fig. 11. Already the as-produced sample shows an interaction zone between Ta and SiC of approx. 1-3 μm. The extension of the interaction layer increases with temperature, being about 2, 9, 18, 33, 33 μm thick after 20 hours tests at 1000, 1200, 1300, 1400, and 1500°C, respectively. The same value for the tests at 1400°C and 1500°C could be related with saturation effects. In addition to the continuous interaction layer, most samples showed areas of increased interaction with a porous, golden-colored reaction product mainly at the inner Ta/SiC interface.
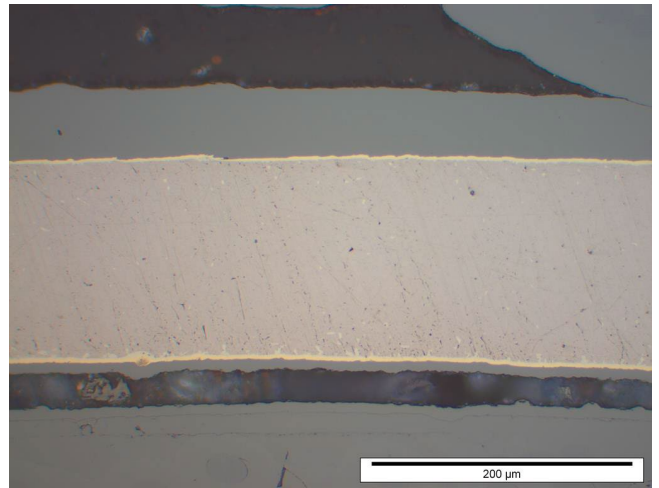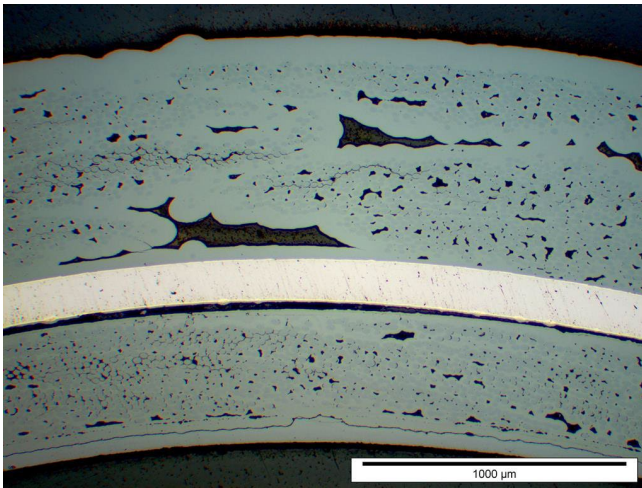
SL2-4, as-received
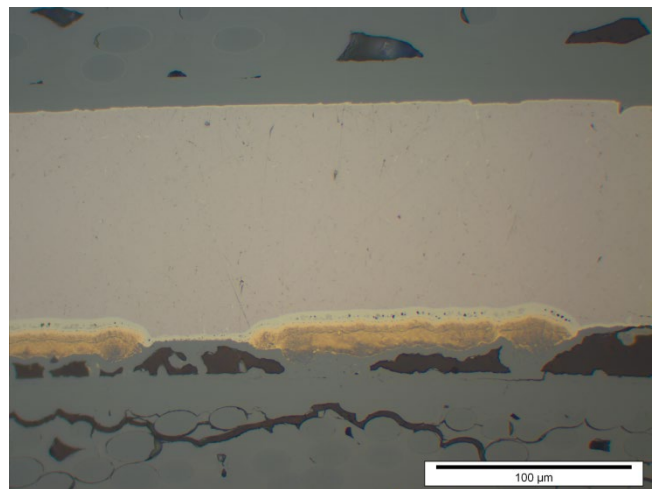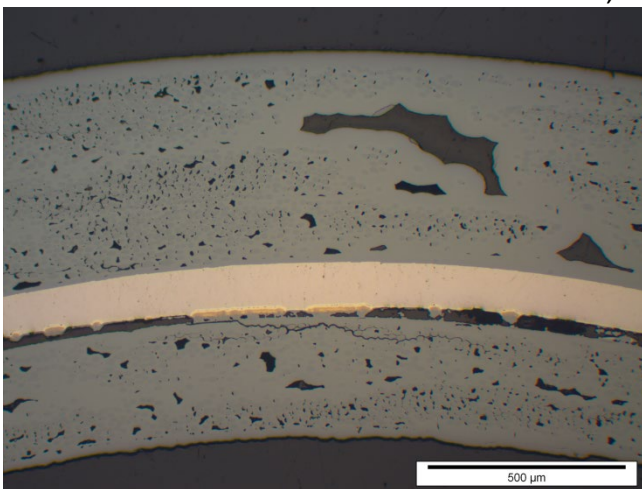
SL3-3, 20h, 1000°C

SL1-1, 20h, 1200°C

SL1-2, 20h, 1300°C

SL1-3, 20h, 1400°C
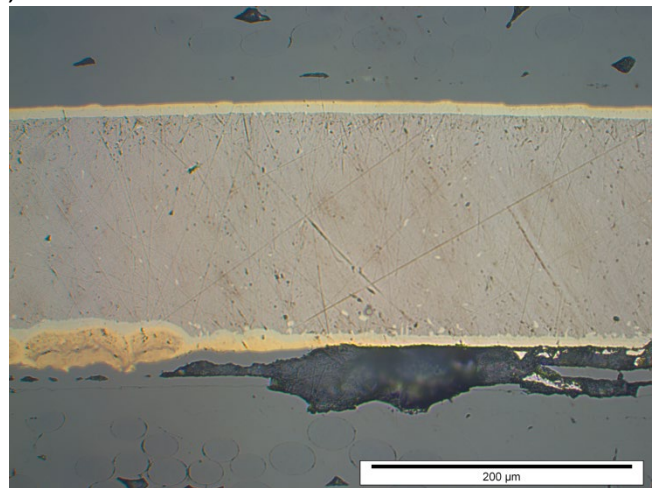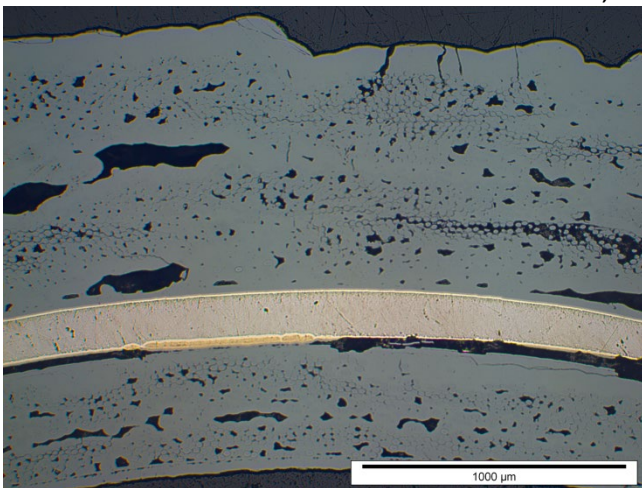
SL1-5, 20h, 1500°C
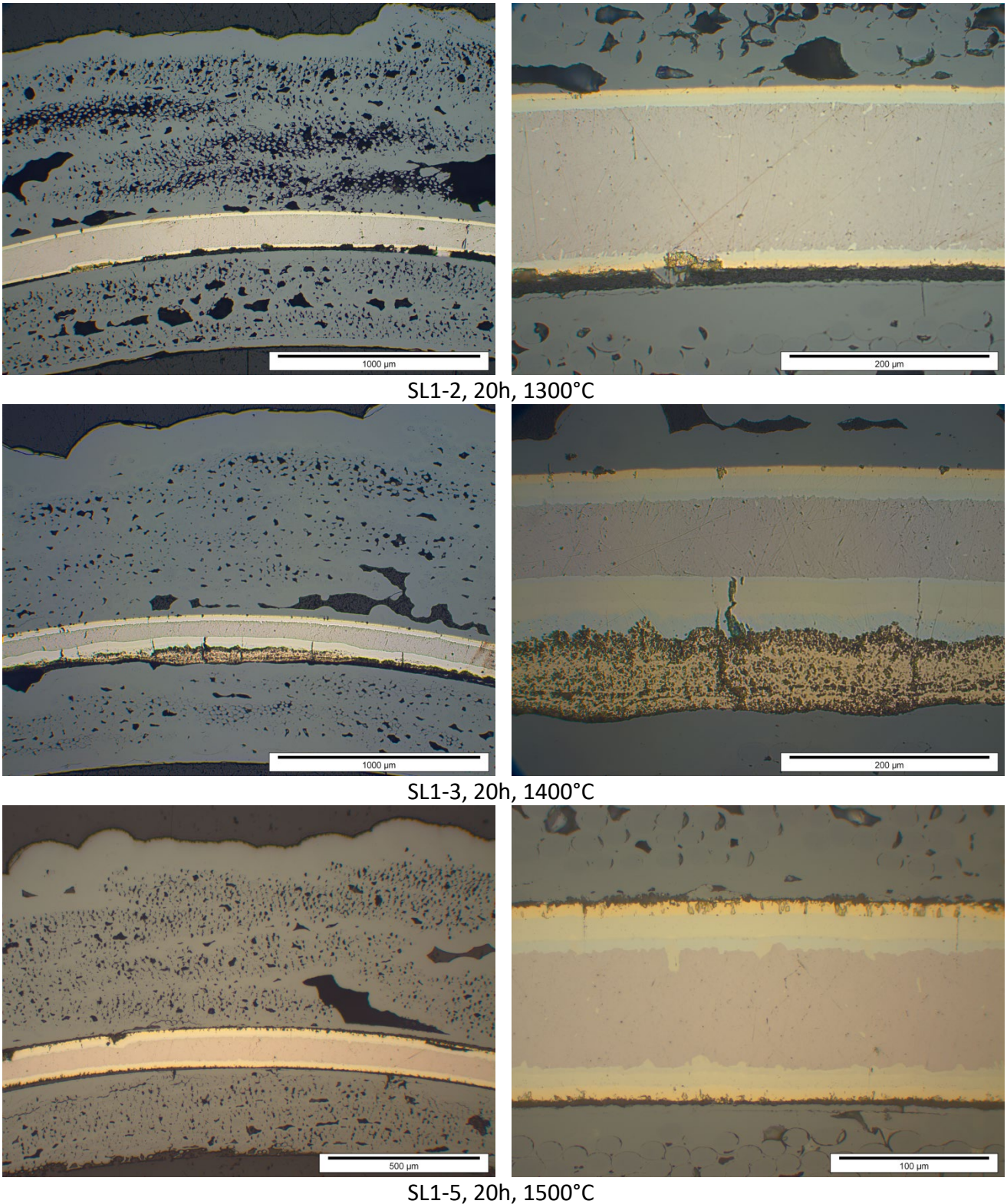
Fig. 11: Optical micrographs of selected sandwich samples' cross sections after oxidation tests in impure helium at various temperatures with focus on the Ta-SiC interaction.

SEM-EDX investigations of the interaction zone provided almost no information due to overlapping of Si-Kα and Ta-M lines. For this reason more sensitive WDX microprobe analyses were

conducted with two specimens annealed at 1400°C and 1500°C. Fig. 12 provides the results of a WDX line scan through the interaction zone of the sample annealed for 3 hours at 1400°C as a typical example for the interactions between SiC and Ta. The layer sequence from silicon carbide bulk to the tantalum bulk material is SiC-TaC_{1-x}-Ta_5Si_3-Ta_2Si-Ta. Pore formation associated with the Kirkendall effect is observed at the tantalum carbide/silicide interface.

| Optical micrograph | BSE image with position of line scan |
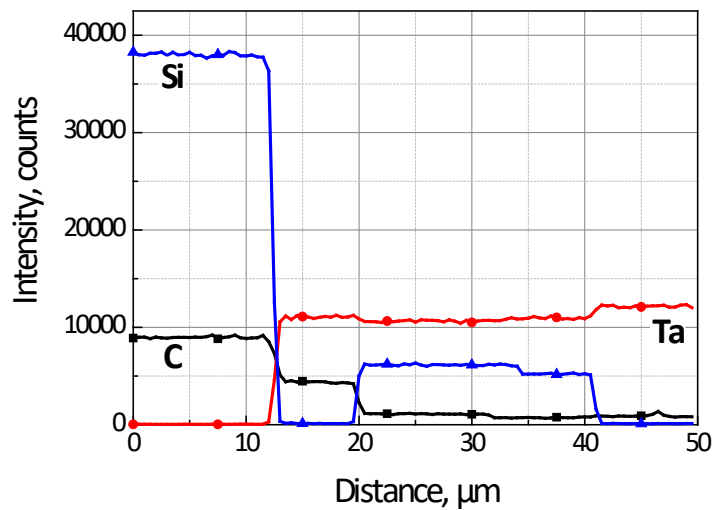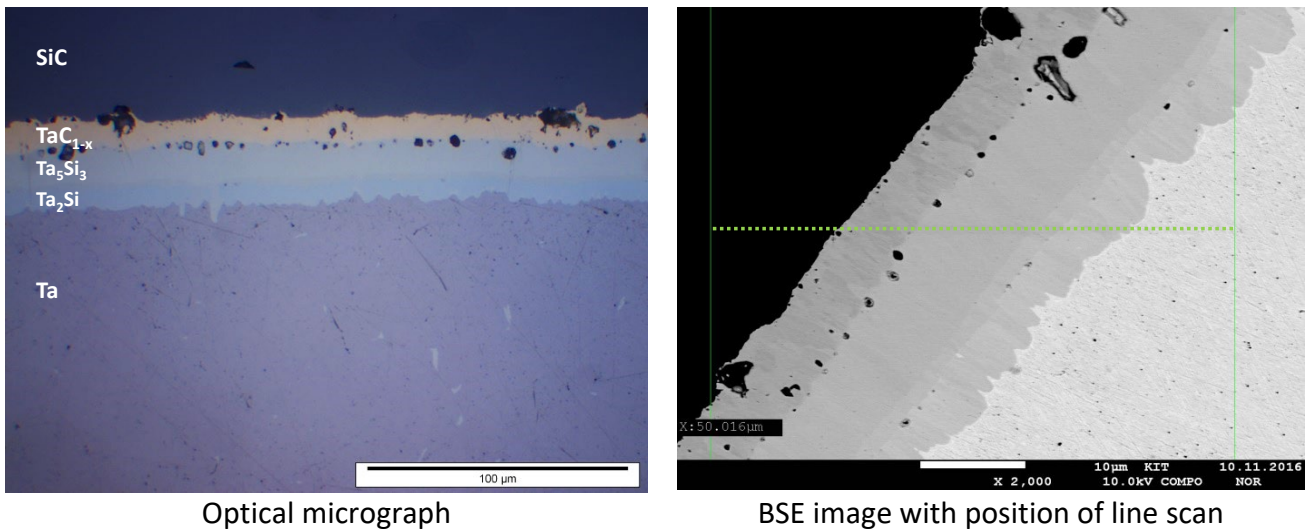
Fig. 12: Qualitative WDX line scan of the Ta-SiC interaction zone of sample SL2-3 annealed for 20 hours at 1400°C.

At 1500°C, an enrichment of carbon between the two tantalum silicide layers was observed. Furthermore, a carbon content of about 5-6 at% was found in the remaining tantalum bulk material for the sample annealed at 1400°C. This is much more than the solubility of carbon in tantalum at this temperature according to the binary phase diagram [20]. The carbon was found in small sub-

μm sized TaC_x particles randomly distributed in the tantalum bulk. Table 4 provides quantitative results of point analyses of the various regions seen in the SEM image (Fig. 12). The porous golden-colored phase seen locally at the inner tantalum tube interaction layer was analyzed to be TaC_{1-x}.

Table 4: WDX analysis results for different regions (see Fig. 12) from Ta to SiC. Mean values of three point measurements each.

	Wt.%				At.%			
	C	Ta	Si	Total	C	Ta	Si	Total
Ta	0.44	98.4	0.06	98.9	6.3	93.3	0.38	100.0
Ta₂Si	0.46	92.7	8.5	101.6	4.5	60.1	35.4	100.0
Ta₅Si₃	0.96	90.0	10.2	101.2	8.5	53.0	38.5	100.0
TaC₁₋ₓ	4.2	91.6	0.03	95.9	41.0	58.8	0.13	100.0
SiC	28.8	0.15	63.2	92.2	51.6	0.02	48.4	100.0

4. DISCUSSION

The most important outcome of this study using GFR prototypic partial pressures of impurities in He coolant, but applying non-prototypic boundary conditions with respect to pressure and flow rate, is the determination of the transition temperature between the passive and active oxidation regimes of SiC-based fuel cladding which occurs at around 1200-1300°C. In the 900-1200°C temperature range all samples showed passive oxidation due to the formation of a protective silica scale connected with very low mass gain that increases with rising temperature. Especially the results obtained at 900°C with very low mass gain during 1000 hour annealing in impure helium indicate that oxidation at operation temperature should not be an issue. The SiC$_f$-SiC samples underwent mass loss due to active oxidation with SiO volatilization from 1300°C and above.

This is a positive result with respect to the potential application of SiC$_f$-SiC CMCs as fuel claddings in gas-cooled fast reactors in which maximum operation temperatures of 900-1000°C are foreseen under nominal conditions. The passive to active transition temperature determined in this study should be valid also for prototypic conditions with respect to pressure and flow rates, because it is mostly dependent on temperature and partial pressure of oxidizing gases [24]. The impurities partial pressures were scaled for these experiments from 70 bar GFR operating pressure to 1 bar applied in these experiments. Hence, the low mass gain rates obtained during passive

oxidation should be representative of the operation conditions. In correspondence with the low mass gains, the silicon oxide scale thicknesses determined in this study were always in the sub-μm range. This is in accordance with literature data [25] [26], where also only SiO_2 layer thicknesses below 1 μm were found for various temperatures and conditions of passive oxidation.

Issues in terms of PyC interphase removal at temperatures below 900°C mentioned in literature [2] have not been observed and are not expected because the dense external SiC layer seems to protect the fibers sufficiently. Fiber attack was only found at the highest temperature of 1600°C.

On the other hand, a strong effect of thermal-hydraulic boundary conditions (pressure, flow rate, gas composition) is expected for active oxidation regime at higher temperature. Hence, the conditions during accident scenarios should be carefully assessed for further analyses of cladding corrosion rates. This is also confirmed by comparison of mass loss data obtained in this study with literature data, as shown in Fig. 13. Dawi [27] and Charpentier [28] obtained much higher mass loss rates of different SiC materials in helium with low oxygen partial pressures (0.2-10 Pa). The oxygen partial pressure is comparable with this study (7 Pa O_2; 20 Pa $O_2+CO_2+H_2O$) but the gas flow rate was higher (10 l/min compared to 30 ml/min in this study). Contrariwise, Terrani [29] measured significantly lower mass loss rates during active oxidation in flowing steam.
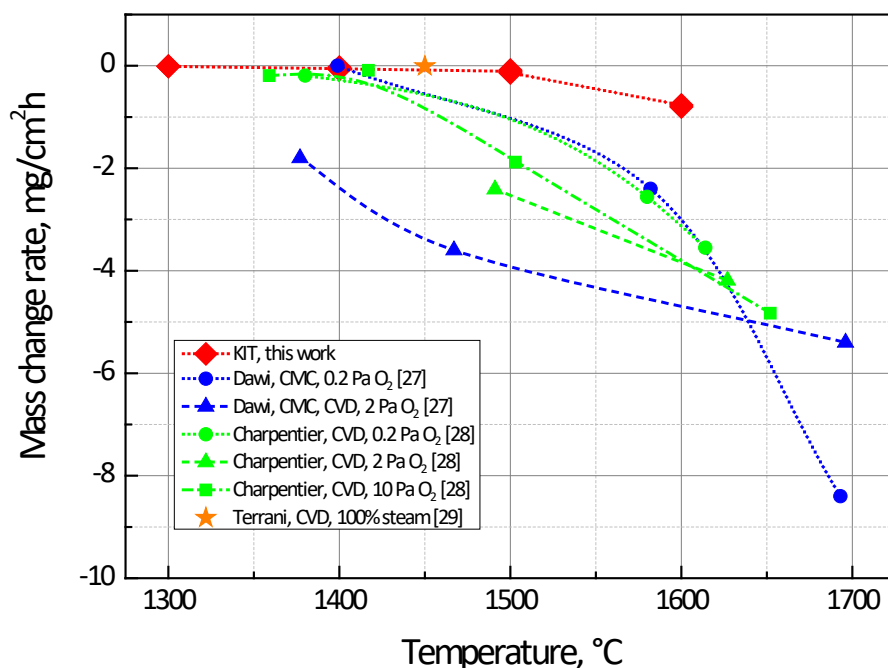
Fig. 13: Mass change rates during active oxidation of SiC materials. Comparison of data obtained in this work with literature data.

The corrosion/recession rates obtained in this study should be a lower limit of expected corrosion rates due to the low gas flow rates and normal pressure applied in the experiments of this study. The conversion of a typical mass loss rate of -0.002 mg/cm^{2}min (found at 1500°C) into the corresponding corrosion thickness rate results in 0.3 μm/h or 7.4 μm/day. Depending on the accident scenario, this value could be acceptable if a wall thickness of approx. 1 mm was employed. On the other hand, higher corrosion rates are expected in real transients due to the more aggressive boundary conditions as well as possible attack of fibers in the bulk of the CMC material, which was almost not observed in the experiments presented in this report.

The total content of oxidant impurities ($O_2+CO_2+H_2O$) of the gas mixture defined in chapter 2.2 corresponds to 0.44 mg/h oxygen. In a first approximation, Eqs.1-4 can be used to calculate the maximum mass gain during passive oxidation, resulting in +0.14 mg/h. The maximum mass loss during active oxidation equals to -0.55 mg/h. These numbers take into account only ideal oxidation behavior and neglect the limitations of the solid-gas heterogeneous reactions. In this study, the maximum mass gain rates measured was 10^{-3} mg/h, meaning that during the tests with passive oxidation starvation conditions for oxidizing gases were by far not reached. Otherwise, the average mass loss rates measured for the test with active oxidation were -0.16 mg/h and -0.70 mg/h at 1400°C and 1500°C, respectively. Hence, at temperature equal to or higher than 1500°C the mass loss rates could not be explained by Eq.4 alone.

As already stated in Fitzgerald's review paper [2], the experimental data basis for high-temperature oxidation under GFR prototypical conditions is very scarce. So it is reasonable to compare the experimental data also with thermodynamic calculations. Fig. 14 gives the results of an equilibrium calculation of 1 mol SiC with 1 mol helium gas with the impurities defined in Table 2. According to this calculation, the transition from the completely stable SiO_2 layer to completely volatile reaction products (passive → active) occurs between 800°C and 1000°C, which is lower than the transition temperature measured in this work. This may be explained by the local conditions at the solid/gas interface differing from the global thermodynamic equilibrium. Kinetic limitations determined by the diffusion of oxidizing gas species to the materials surface and the outwards diffusion of gaseous oxidation and volatilization products are not considered in the calculations. This is probably leading to the observed shift of the active → passive transition to higher temperatures.

Further thermodynamic calculations were done for the Ta-SiC interaction. As seen in the experiments, the calculations confirm that tantalum and silicon carbide are chemically not

compatible with each other. Tantalum carbides and tantalum silicides are the stable reaction products. According to the results of the calculation shown in Fig. 15, a complex multiphase interaction zone containing various carbides and silicides is formed between SiC and tantalum. The experimentally observed phase sequence is in accordance with the tie lines of the isothermal section. Additionally, the temperature-composition diagram reveals the lowest eutectic temperature of 1842 °C on the SiC-rich side of the SiC-Ta system. In the experiments, sub-stoichiometric TaC_{1-x} as well as Ta_5Si_3 and Ta_2Si were found in the interaction layer which is, also in the order of their appearance, in good agreement with the calculation results. The phase diagram Ta-C [20] reveals hypo-stoichiometry of the "TaC" phase which is confirmed by the microprobe elemental analyses.
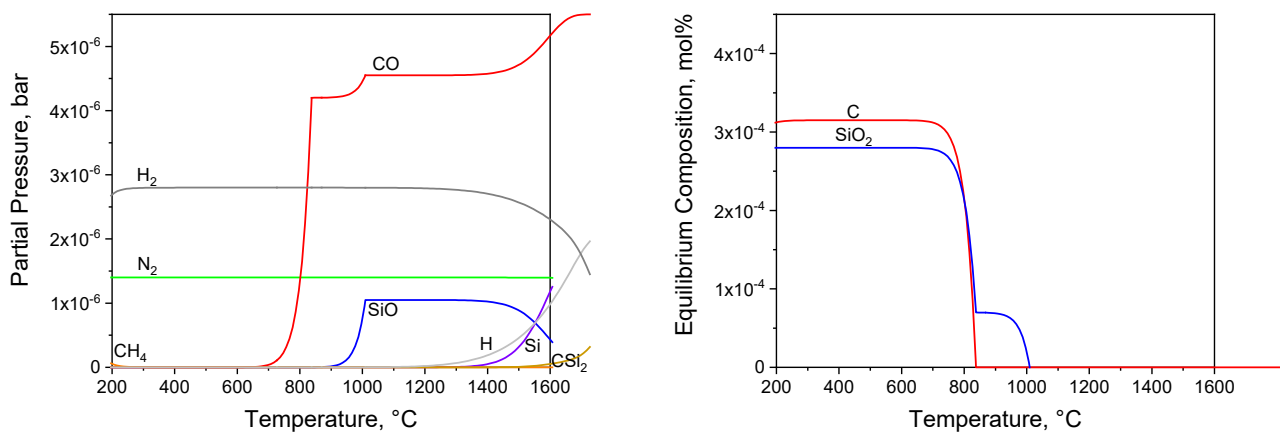
Fig. 14: Thermodynamic calculation with Thermo-Calc [14] of composition of gas phases (left) and solid phases (right) with 1 mol SiC and 1 mol helium with impurities according to Table 2 versus temperature.

It is not clear to which extent the SiC-Ta interaction affects the function of the tantalum hermeticity liner in the composite cladding. Mechanical and leak tightness tests, as well as longer experiments especially under operation conditions, are necessary to resolve this issue. In any case, the contact of tantalum with the oxidizing atmosphere has to be avoided because of the rapid oxidation kinetics of the metal as seen qualitatively for non-protected edge areas of the sandwich samples especially at lower temperatures. This is in accordance with results obtained recently by Avincola [30], who found during oxidation of tantalum in argon-steam mixtures the formation of more stable oxide films only from temperatures beyond 1000°C. One of the main reasons for the formation of non-protective oxide scales is the high Pilling-Bedworth ratio of 2.47 for the formation

of Ta_2O_5. Stress relief due to plastic deformation in the base metal as well as in the oxide layer should be the reason for the formation of protective oxide layers at higher temperatures.

Similar layer-wise interaction zones with the formation of carbides and silicides have been found recently for the system Zircaloy-4/SiC by Grosse [31]. There the interaction layer was even more complex due to the presence of tin resulting in a quaternary system.
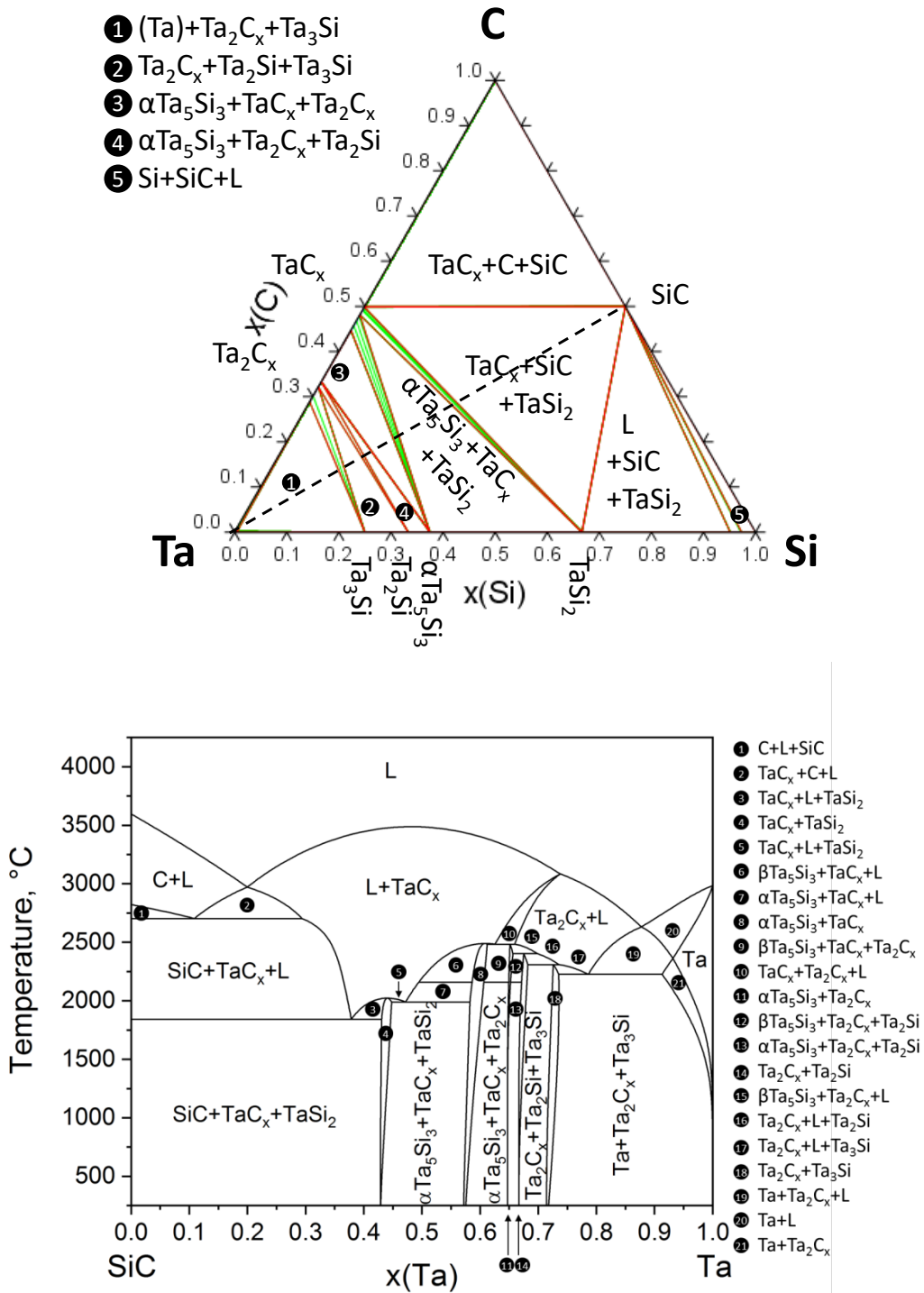
Fig. 15: Calculated isothermal section in the ternary Ta-Si-C system at 1500 °C (top) and temperature-composition diagram across the SiC-Ta interface (bottom).

5. SUMMARY AND CONCLUSIONS

The oxidation of SiC_f-SiC cladding tube segments and sandwich tubes with inner tantalum layer in impure helium atmosphere prototypical for GFRs was investigated at normal pressure in the temperature range between 900°C and 1600°C using a thermogravimetric device. The composition of the gas mixture (helium plus H_2O, H_2, CO, CO_2, N_2, O_2, CH_4) was defined according to a literature survey by NNL performed in the framework of the MatISSE project [2]. The partial pressures of the impurities were scaled to normal pressure applied in these experiments.

The transition from passive oxidation (formation of a protective silica scale) to active oxidation (volatilization of SiO and other gaseous species) occurred between 1200°C and 1300°C. Hence, during target operational temperatures of 900-1000°C the SiC_f-SiC CMC cladding material should withstand long-term operation with respect to oxidation and corrosion. It is expected that the results in the passive oxidation region can be extrapolated to GFR conditions because the oxidation rates are mainly dependent on temperature and oxygen partial pressure which were prototypic in the tests presented in this paper. At temperature higher than 1200°C, i.e. under accident conditions, volatilization of components would lead to degradation of the SiC based cladding tubes. Because of the strong dependence of the active oxidation on the thermo-hydraulic boundary conditions more experiments under prototypic conditions regarding gas flow rates and pressure are needed and have been partially conducted in the framework of the MatISSE project.

An Arrhenius type kinetic rate equation was developed for the linear volatilization rates at high temperatures. The mass gains during passive oxidation were too low during the applied annealing times (20-1000 hours) to develop a reasonable rate correlation for the passive oxidation.

The oxidation test results of sandwich tube segments could not be used for deriving kinetic correlations because of partial oxidation of non-protected tantalum at the edges of the samples. However, these tests highlighted the severe interactions occurring between SiC and Ta, leading to the formation of tantalum silicides and carbides. The influence of these interactions on the hermeticity of the sandwich cladding tubes is still an open issue which needs to be addressed in future.

The experiments were compared to the scarce literature data available showing agreement for the passive oxidation but strong scatter of data in the active oxidation range. Thermodynamic equilibrium calculations supported and confirmed the experimental results.

The results obtained in this study at normal pressure and low gas flow rates will be compared with results obtained in helium loops at CV Rez with prototypic pressure and gas flow rates, to be published elsewhere.

DATA AVAILABILITY

The raw/processed data required to reproduce these findings cannot be shared at this time due to legal reasons.

REFERENCES

[1] Pierre-François Giroux. (2017) MatISSE project. [Online]. http://www.fp7-matisse.eu/

[2] K. Fitzgerald and D. Shepherd, "Review of SiCf/SiCm corrosion, erosion and erosion-corrosion in high temperature helium relevant to GFR conditions," *Journal of Nuclear Materials*, vol. 498, pp. 476-494, 2018.

[3] V. Angelici Avincola et al., "High-temperature tests of silicon carbide composite cladding under GFR conditions," *Energy Procedia*, vol. 127, pp. 320-328, 2017.

[4] T. Goto and H. Homma, "High-temperature active/passive oxidation and bubble formation of CVD SiC in O2 and CO2 atmospheres," *Journal of the European Ceramic Society*, vol. 22, pp. 2749-2756, 2002.

[5] N. Jacobson, B. Harder, and D. Myers, "Oxidation transitions for SiC part I. Active-to-passive transitions," *Journal of the American Ceramic Society*, vol. 96, pp. 838-844, 2013.

[6] B. Harder, N. Jacobson, and D. Myers, "Oxidation transitions for sic part II. Passive-to-active transitions," *Journal of the American Ceramic Society*, vol. 96, pp. 606-612, 2013.

[7] E.J. Opila, "Oxidation and volatilization of silica formers in water vapor," *Journal of the American Ceramic Society*, vol. 86, pp. 1238-1248, 2003.

[8] V. Angelici Avincola, D. Cupid, and H.J. Seifert, "Thermodynamic modeling of the silica volatilization in steam related to silicon carbide oxidation," *Journal of the European Ceramic*

Society, vol. 35, pp. 3809-3818, 2015.

[9] L. Filipuzzi, G. Camus, R. Naslain, and J. Thebault, "Oxidation Mechanisms and Kinetics of 1D-SiC/C/SiC Composite Materials: I, An Experimental Approach," *Journal of the American Ceramic Society*, vol. 77, pp. 459-466, 1994.

[10] C.F. Windisch Jr., Henager Jr. C.H., G.D. Springer, and R.H. Jones, "Oxidation of the carbon interface in nicalon-fiber-reinforced silicon carbide composite," *Journal of the American Ceramic Society*, vol. 80, pp. 569-574, 1997.

[11] SETARAM Instrumentation. TAG (Thermogravimetric Analysis). [Online]. https://www.setaram.com/setaram-products/thermal-analysis/tag/

[12] ZIROX - SENSOREN & ELEKTRONIK GmbH. Oxygen Analyzer SGM5. [Online]. https://www.zirox.de/en/products/analyzers/oxygen-analyzer-sgm5.html

[13] L. Chaffron et al., "Innovative SiC/SiC composite for nuclear applications," in *EPJ Web of Conferences 51, Art. No. 01003*, 2013.

[14] J. O. Anderson, T. Helander, L. Höglund, P. F. Shi, and B. Sundman, "Thermo-Calc and DICTRA, Computational tools for materials science," *Calphad 26*, pp. 273-312, 2002.

[15] Scientific Group Thermodata Europe (SGTE). [Online]. http://www.sgte.org

[16] H. L. Lukas, S. G. Fries, and B. Sundman, *Computational Thermodynamics - The CALPHAD Method*. Cambridge: Cambridge University Press, 2007.

[17] J. Gröbner, H. L. Lukas, and F Aldinger, "Thermodynamic Calculation of the Ternary System Al-Si-C," *Calphad 20 (2)*, pp. 247-254, 1996.

[18] H. Mao, M. Selleby, and O. Fabrichnaya, "Thermodynamic reassessment of the Y2O3-Al2O3-SiO2 system and its subsystems," *Computer Coupling of Phase Diagrams and Thermochemistry 32*, pp. 399-412, 2008.

[19] Z. Guo, W. Yuan, Y Sun, Z. Cai, and Z. Qiao, "Thermodynamic Assessment of the Si-Ta and Si-W Systems," *Journal of Phase Equilibria and Diffusion 30*, pp. 564-570, 2009.

[20] K. Frisk and A. Fernandez Guillermet, "Gibbs energy coupling of the phase diagram and thermochemistry in the tantalum-carbon system," *Journal of Alloys and Compounds 238*, pp. 167-179, 1996.

[21] J.C. Schuster, "Investigations in the ternary systems V-Si-C and Ta-Si-C," *J. Chim. Phys.*, vol. 90, pp. 373-378, 1993.

[22] M. Naka, Feng, J.C., and J.C. Schuster, "Phase Reaction and Diffusion Path of the SiC/Ti System," *Metallurgical and Materials Transactions A*, vol. 28A, pp. 1385-1390, 1997.

[23] T. Laurilla, K. Zeng, J. K. Kivilahti, J. Molarius, and I. Suni, "TaC as a diffusion barrier between Si and Cu," *Journal of Applid Physics 91*, pp. 5391-5399, 2002.

[24] B. Schneider, A. Guette, R. Naslain, M. Cataldi, and A. Costecalde, "A theoretical and experimental approach to the active-to-passive transition in the oxidation of silicon carbide: Experiments at high temperatures and low total pressures," *Journal of Materials Science*, vol. 33, pp. 535-547, 1998.

[25] C.E. Ramberg, G. Cruciani, K.E. Spear, and R.E. Tressler, "Passive oxidation kinetics of high-purity silicon carbide from 800°C to 1100°C," *Journal of the American Ceramic Society*, vol. 79, pp. 2897-2911, 1996.

[26] S. Nogami et al., "Oxidation behavior of SiC/SiC composites for helium cooled solid breeder blanket," *Fusion Engineering and Design*, vol. 83, pp. 1490-1494, 2008.

[27] K. Dawi, M. Balat-Pichelin, L. Charpentier, and F. Audubert, "High temperature oxidation of SiC under helium with low-pressure oxygen. Part 3: Beta-SiC-SiC/PyC/SiC," *Journal of the European Ceramic Society*, vol. 32, pp. 485-494, 2012.

[28] L. Charpentier et al., "High temperature oxidation of SiC under helium with low-pressure oxygen. Part 2: CVD beta-SiC," *Journal of the European Ceramic Society*, vol. 30, pp. 2661-2670, 2010.

[29] K.A. Terrani et al., "Silicon carbide oxidation in steam up to 2 MPa," *Journal of the American Ceramic Society*, vol. 97, pp. 2331-2352, 2014.

[30] V. Angelici Avincola, M. Janek, U. Stegmaier, M. Steinbrück, and H.J. Seifert, "Tantalum Oxidation in Steam Atmosphere," *Oxidation of Metals*, vol. 85 , pp. 459-487, 2016.

[31] M.K. Grosse et al., "High temperature interaction of SiC and Zry-4," in *Proceedings of the 2018 International Congress on Advances in Nuclear Power Plants, ICAPP 2018*, Charlotte, NC, USA, 2018, pp. 590-597.